Rodríguez-Rodríguez, H.; Salas, G.; Arias-Gonzalez, JR. (2020). Heat Generation in Single Magnetic Nanoparticles under Near-Infrared Irradiation. The Journal of Physical Chemistry Letters. 11(6):2182-2187. https://doi.org/10.1021/acs.jpclett.0c00143

Heat Generation in Single Magnetic Nanoparticles under Near Infrared Irradiation

Héctor Rodríguez-Rodríguez,[1,2] *Gorka Salas,*[1,3,*] *and J. Ricardo Arias-Gonzalez*[4,*]

[1]Instituto Madrileño de Estudios Avanzados en Nanociencia (IMDEA-Nanoscience), Cantoblanco 28049, Madrid, Spain

[2]Departamento de Química-Física Aplicada, Universidad Autónoma de Madrid, 28049 Cantoblanco, Madrid, Spain

[3]CNB-CSIC-IMDEA Nanociencia Associated Unit "Unidad de Nanobiotecnología", Madrid, Spain

[4]Centro de Tecnologías Físicas, Universitat Politècnica de València, Camino de Vera s/n, 46022 Valencia, Spain

*Corresponding Author: ricardo.ariasgonzalez@upv.es,

ricardo.ariasgonzalez@gmail.com, gorka.salas@imdea.org

ABSTRACT

Heat generation by point-like structures is an appealing concept for its implications in nanotechnology and biomedicine. The way to pump energy that excites heat locally and the synthesis of nanostructures that absorb such energy are key issues in this endeavor. High-frequency alternate magnetic or near-infrared optical fields are used to induce heat in iron oxide nanoparticles, a combined solution that is being exploited in hyperthermia treatments. However, the temperature determination around a single iron oxide nanoparticle remains a challenge. We study the heat released from iron oxide nanostructures under near-infrared illumination on a one-by-one basis by optical tweezers. To measure the temperature, we follow the medium viscosity changes around the trapped particle as a function of the illuminating power, thus avoiding the use of thermal probes. Our results help interpreting temperature, a statistic parameter, in the nanoscale and the concept of heat production by nanoparticles under thermal agitation.

TOC Graphic.

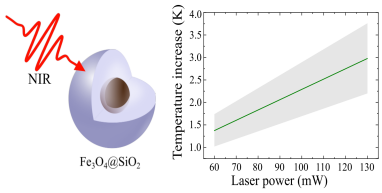

KEYWORDS

Heat, nanoparticle, optical tweezers, iron oxide, magnetic, hyperthermia

The use of nanoparticles (NPs) that generate heat under external stimuli is the subject of extensive research because they promote engineering at the nanoscale and enable several physical-chemical activities compatible with life.[1] In biomedicine, especial attention is devoted to NPs whose hyperthermia capacity can be controlled non-invasively and remotely by optical and magnetic fields, killing tumor cells by increasing their temperature.[2-3]

Among other materials, iron oxide-based magnetic NPs (IONPs) commonly display low toxicity and their magnetic properties are useful for contrast enhancement in magnetic resonance imaging. They release heat under appropriate alternating (AC) magnetic fields[4-5] and, as a matter of fact, a fair number of clinical trials have been or are being conducted.[6-9] In recent years, the optical absorption shown by magnetic nanostructures and subsequent heat production has come into play as an alternative method to perform hyperthermia with IONPs. In particular, the use of near infrared (NIR) irradiation and its potential to treat tumors through the heat generated at the IONPs have been demonstrated.[10-20] This method is gaining interest due the low absorption and dispersion of physiological tissues at NIR wavelengths.[21-22] AC magnetic fields are more advantageous than NIR irradiation from the point of view of tissue penetration, but a NIR laser is a more affordable technology than an AC magnetic field generator and requires lower doses than those for magnetic hyperthermia.[23] For these reasons, both optical and magnetic hyperthermia complement each other in thermal ablation clinical applications.[11]

Knowledge of the temperature rise produced by a single NP at its vicinity is a crucial step forward in the understanding of the local heating caused by remotely activated NPs. However, in spite of the large efforts dedicated to hyperthermia treatments to date, the quantification of the heat released from IONPs is routinely performed through bulk temperature measurements on samples typically containing 10^{12}–10^{15} NPs.[24-26] Exceptional studies on temperature increment

determination at the single particle level have only been performed on Au NPs with the use of calibrated probes in contact with the heating nanostructures.[27-28]

In this work, iron oxide nanocrystals (IONPs) were encapsulated in silica to yield near-spherical stratified silica-coated iron oxide (IONP@SiO_2) nanostructures (Supporting Information). The silica shell facilitates their dispersion in water and enhances gradient forces in the optical trap; in fact, tridimensional optical trapping of bare IONPs was not possible under our experimental conditions, as detailed in our previous work.[29] TEM examination before and after encapsulation (Supporting Information and Fig. S1) revealed mean ± SD sizes of 11 ± 1 nm and 99 ± 3 nm, respectively.

The Fe_3O_4 core is an excellent candidate for optical heating because magnetite immersed in water approaches the absorption behavior of a black body in the visible and NIR spectral ranges.[30] The complex refractive index, $n = n' + in''$, of Fe_3O_4[31] relative to water ($n' \gtrsim 1.6$) enables transparency and a moderate refracting power, in contrast to gold ($n' \sim 10^{-1}$),[32] which mostly reflects and scatters light at off-plasmon resonance conditions.[33] The imaginary part (relative to water), $n'' \gtrsim 0.4$, is low but not negligible, which allows a high wave penetration depth in the magnetic material while enhancing energy absorption. This is in sharp contrast to gold, $n'' \gtrsim 1.5$, in which light energy hardly crosses the surface (off-resonance conditions).

These behaviors exhibited by magnetite are not strongly dependent on the wavelength in the visible and NIR ranges. This is reflected in the absorption cross section, which tends to be flat with the wavelength and does not present Mie resonances. The theoretical absorption (σ_{abs}), scattering (σ_{sc}) and extinction ($\sigma_{ext} = \sigma_{abs} + \sigma_{sc}$) cross sections of a single IONP@SiO_2 nanostructure in water are shown in Fig. 1, along with the absorption cross section for the bare IONP in air. Simulations have been generated by using exact calculations based on the extension

of Mie theory for stratified spheres.[34-36] As expected, the extinction cross section profile of IONP@SiO_2 nanostructures shows good agreement with the bulk attenuance measurement (Fig. 1).

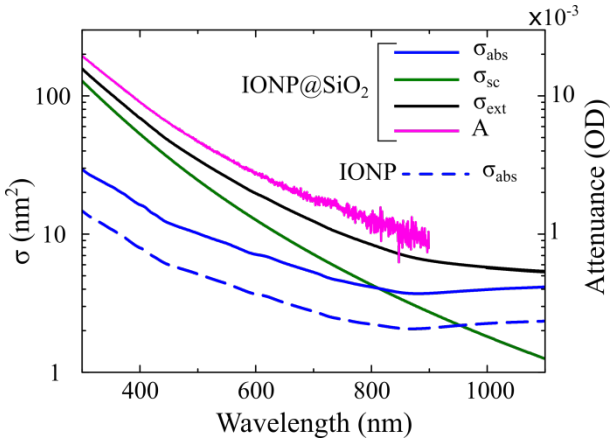

Figure 1. Optical cross sections. Absorption (σ_{abs}, blue), scattering (σ_{sc}, green) and extinction (σ_{ext}, black) cross section of a single IONP@SiO_2 nanostructure in water and σ_{abs} of a single uncoated IONP (dash blue) in air, as calculated from Mie theory. The experimental bulk attenuance (A) of an ensemble of IONP@SiO_2 nanostructure in water is shown in pink in optical density units.

The absorption cross section of IONP@SiO_2 nanostructures in water is near 8 times greater than that of similar Au@SiO_2 nanostructures of equal stratified sizes in water. It is also remarkable that the absorption cross section of the bare IONP core nearly doubles after silica encapsulation and water immersion, being $\sigma_{abs} = 4.0$ nm^2 at the trapping laser wavelength $\lambda = 808$ nm for IONP@SiO_2 nanostructures in water. The absorption cross section of the bare IONP in water is 3.6 nm^2, still smaller than the whole nanostructure. The thick, highly curved silica shell thus has the effect of a lens that concentrates light onto the magnetic core.

Radiative effects were negligible in our optical configuration and for the particles used in our experiments (Supporting Information and Fig. S2) and, therefore, light absorption by the NPs in the trap was assumed to be ultimately released via thermal dissipation.

The stochastic dynamics of single silica-coated magnetic NPs in the trap was stationary, within a harmonic potential well, as characterized in Fig. S3 (a) by the power spectral density of fluctuations,[29, 33, 37-41] and stable for minutes. The limiting frequency at which the NP explores the focal region, the so called corner frequency, increases with the laser power, Fig. S3 (b), a consequence of both increasing trap stiffness with power and decreasing viscosity of the surrounding water with power due to heating from the magnetic NP.

Since there are no additional energy dissipation mechanisms, the heat generation from the particle equals the absorbed power:

$$\dot{q} = P_{abs} \, . \tag{1}$$

The temperature increase around the magnetic core is calculated by solving Fourier's law for heat conduction (as detailed in the Supporting Information, including Fig. S4):

$$\Delta T(r) = T(r) - T_0 = \begin{cases} \dfrac{P_{abs}}{4\pi C_w r} \, , & r \geq a \qquad \text{(2a)} \\ \dfrac{P_{abs}}{4\pi C_{sa} r} + \dfrac{P_{abs}}{4\pi a}\left(\dfrac{1}{C_w} - \dfrac{1}{C_{sa}}\right) , & a_c \leq r \leq a \qquad \text{(2b)} \end{cases}$$

where T is the absolute temperature (r, the radial coordinate from the center of the NP) and T_0 is the absolute room temperature; a_c and a are the radius of the core IONP and the whole IONP@SiO_2 nanostructure, respectively; and C_{sa} and C_w are the thermal conductivities of silica and water, respectively. The power absorbed by the nanostructure, P_{abs}, requires of a particular treatment since the particle is much smaller than the focal region and not static in the trap (Supporting Information, including Figs. S5 and S6):

$$P_{abs} = P_{trap}\frac{\kappa_\rho\sqrt{2\kappa_z}\sigma_{abs}}{\sqrt{\pi^3 k_B T}}\int_{-\infty}^{+\infty} dz \frac{\exp\left(-\frac{\kappa_z z^2}{2k_B T}\right)}{\kappa_\rho W_0^2[1+(z/z_0)^2]+4k_B T} \ . \quad (3)$$

We calculated the increase in temperature around an IONP@SiO_2 nanostructure at different laser powers (Fig. S6). The thermal conductivity of the shell does not affect the temperature outside the NP, Eq. (2a), although, as explained in the previous section, the power absorbed by the magnetic core does depend on the lens effect produced by the silica shell.

For many materials and phototherapies, laser-induced effects only depend linearly on the laser power. For optical hyperthermia treatment designs, which often differ in the laser power used, the heating coefficient is a very convenient parameter to compare, across light-based methodologies, the temperature rise per watt in a nanostructure. This parameter depends on the shape and composition of the nanostructure, and modifies in the presence of nearby nanostructures, but its value affords predictions on the heating behavior of particles. In the following, we experimentally define and measure the laser-heating coefficient of the magnetic NPs, with which comparisons between theory and experiment will be established. IONP@SiO_2 nanostructures were flowed in a microfluidics chamber (Supporting Information) showing good colloidal stability and dispersion in water. Optical confinement of both single IONP@SiO_2 nanostructures and groups of a small number of NPs bunched in the optical trap (*IONP@SiO_2 clusters* from now on[39]) were performed as described in our previous work.[29] The particle concentration was sufficiently low to prevent interference signals from successive trapping events.

In order to measure heat generation in single IONP@SiO_2 nanostructures, we studied the viscosity change in the surrounding water as the trapping power was varied (Supporting Information). We performed Stokes' law assays for powers ranging from 60 to 120 mW,[29, 39-40]

obtaining the drag coefficient, γ, as a function of the power in the trap. Representative results from these experiments are shown in Fig. 2 (a). A decay trend in γ is observed with increasing power, Fig. 2 (b), which reveals a decrease in viscosity of the medium as a consequence of heat dissipation from the NP.

The functional relation between the temperature and the power in the trap is normally expressed as $T(P_{trap}) = T_0 + B \times P_{trap}$, where B is the laser-induced heating coefficient.[42] When a single absorbing particle in the trap is much smaller than the focal region, $\Delta T / P_{trap}$ cannot be considered constant because the power absorbed by the particle is position-dependent. As explained in the Supporting Information, the temperature rise approximately squares with the trap power at low power, which makes the heating coefficient depend on the trap power too. However, the absorbed power can be considered linear with the trap power above some 20 mW in our experimental configuration because the particle remains near the center of the focal region most of the time (Fig. S5). The friction coefficient in these conditions is

$$\gamma(P_{trap}) = 3\pi d_{hydro} \eta(T_0 + B \times P_{trap}), \quad (4)$$

where d_{hydro} is the hydrodynamic diameter of the trapped particle and $\eta(T)$ the temperature-dependent viscosity of the medium.

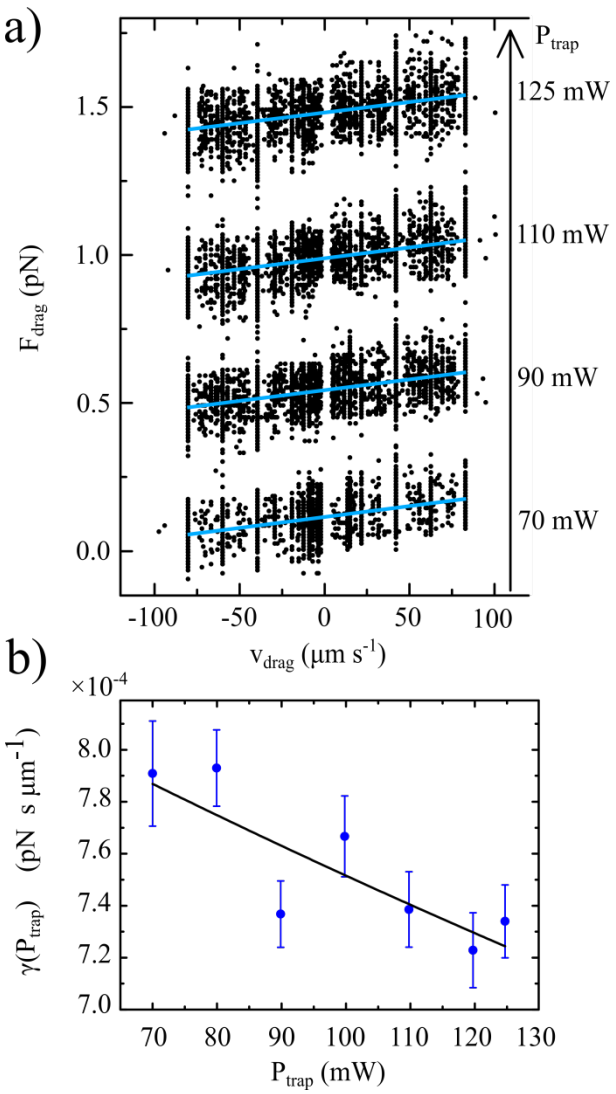

Figure 2. Experimental determination of the temperature. (a) Drag force versus velocity for a single IONP@SiO_2 nanostructure confined at four representative trap powers. Data have been artificially shifted in the vertical axis for the sake of clarity (note that $F_{drag}(v_{drag} = 0) = 0$). Blue curves are linear fits revealing the drag coefficient of the particle, γ. **(b)** Drag coefficient of a single IONP@SiO_2 nanostructure as a function of the power in the trap. Black curve is the optimal fitting to $\gamma(P_{trap}) = 3\pi d_{hydro}\eta(T_0 + B \times P_{trap})$. The parameters obtained from this sample particle were $d_{hydro} = 113 \pm 3$ nm and $B = 34.1 \pm 0.7$ K·W^{-1}.

Equation (4) was fitted to the experimental data to obtain corresponding heating coefficients and d_{hydro}. Since the particles are approximately spherical (Fig. S1) and their size do not change for temperature increments of a few degrees, d_{hydro} approaches the size of the IONP@SiO_2 nanostructure when a single particle is in the trap. Single and multiple trapping events are plotted in Fig. 3 (raw data for each trapping event is provided in the Supporting Information). The analysis of the set of particles measured on a one-by-one basis yielded $B = 23 \pm 6$ K·W^{-1} (mean ± SD). This laser-heating factor is much higher than that of purely dielectric particles considering that water absorption by our 808-nm laser is marginal.[42-43] Indeed, the laser-induced heating coefficients of water comply with $B_w < 3$ K·W^{-1} and the temperature rise keeps $\Delta T_w < 0.3$ K at $P_{trap} = 100$ mW (Supporting Information). Our experimental results are consistent with these theoretical predictions: measurements of the laser-heating coefficient for individual 1-μm polystyrene beads yielded $B_{PS} = 4 \pm 1$ K·W^{-1} (mean ± SD) and $\Delta T_{PS} = 0.4$ K at $P_{trap} = 100$ mW (Fig. 3).

Single IONP@SiO_2 nanostructures yield $\Delta T = 2.3 \pm 0.6$ K under laser pumping such that $P_{trap} = 100$ mW (Fig. 3). The theoretical prediction (see Eq. (3)), without considering the water absorption contribution, is of $\Delta T = 2.3$ K at the SiO_2 surface (Fig. S6). The extrapolation of this result to the surface of the IONP core implies that a weakly focused trapping beam in the NIR induces a temperature rise of $\Delta T = 14$ K with an optical power of 100 mW.

The heating efficiency exhibited by the herein analyzed IONP cores exceeds that of Au NPs, as compared to earlier studies at off-resonance conditions. In particular, the ratio [heating coefficient]/[geometric cross section] measured on the surface of an Au NP in equivalent optical trapping conditions was around 9 times lower than the corresponding ratio for an IONP.[33] Similar results were obtained by Bendix et al.,[27] where this ratio was around 5 times lower than that of the

herein considered IONPs, despite the optical power in the trap in that study was more concentrated (higher numerical aperture, higher intensity) than in our setup.

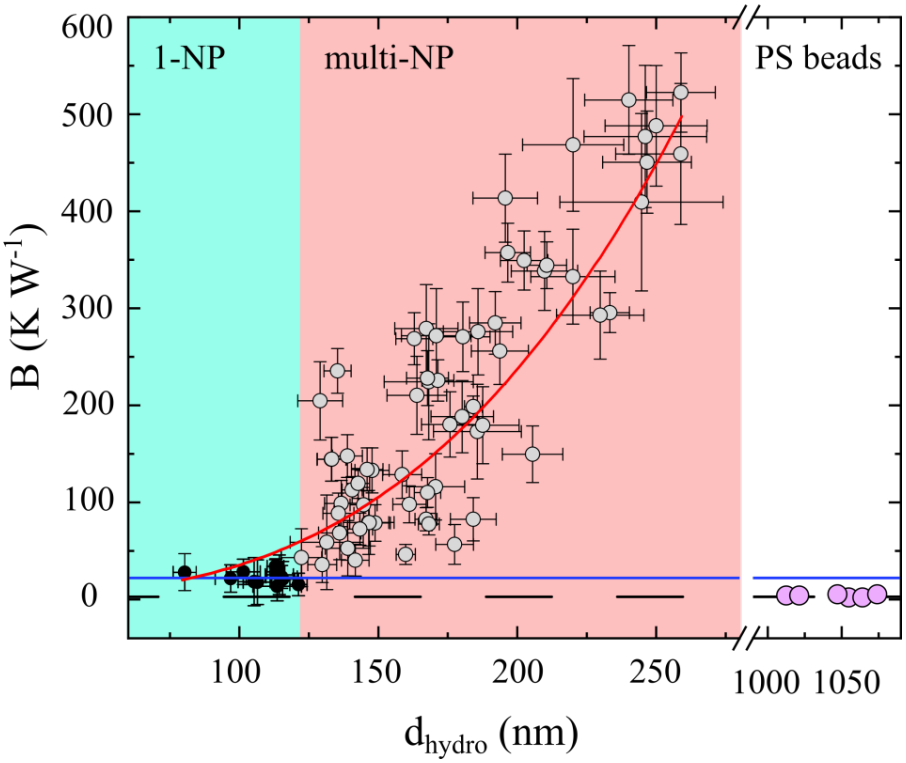

Figure 3. Temperature measurements near magnetic nanostructures. The laser heating coefficient is shown for a set of 14 single IONP@SiO_2 nanostructures and near 70 IONP@SiO_2 clusters of varying hydrodynamic diameter measured at $P_{trap} = 100$ mW. The blue-shaded area indicates the single IONP@SiO_2 nanostructure diameter range, as derived from TEM measurements. The horizontal blue line is the average temperature increase of single IONP@SiO_2 nanostructures. Data within the red-shaded area correspond to IONP@SiO_2 clusters and the red curve is a fitting of all the measurements (single IONP@SiO_2 and clusters) to $\sim d_{hydro}^{n}$. Purple dots are control experiments performed with 1 μm-diameter polystyrene (PS) beads. The black, dashed line marks the temperature increase of distilled water under identical conditions.

With regards to the IONP@SiO_2 clusters, it is observed in Fig. 3 that ΔT increases with the size of the trapped object.[44] Due to the geometry and orientation of the small number of particles in each cluster against the viscous drag, it is not possible to determine the exact number of particles at the focal region on each assay. However, by fitting our results to a power law, $\Delta T \sim d_{hydro}^{n}$, we find $n = 2.9 \pm 0.2$, consistent with a coarse-grained model in which the temperature rise scales with the volume of the optically generated IONP@SiO_2 aggregate. The third law behavior of the heat coefficient with the size of the IONP@SiO_2 clusters can be used as a reference when considering aggregation inside cells. However, it is important to note that these clusters, apart from containing silica, hold gaps between IONP@SiO_2 nanostructures filled with water molecules. The heat coefficient for a magnetite nanoparticle does not necessarily increase with its volume because it actually depends on the absorption optical cross section of the nanoparticle, which is not linear with the volume of the nanoparticle. The herein measured heating coefficients for individual clusters, which scale up to 10^2-10^3 $K \cdot W^{-1}$ for hydrodynamic sizes in the 10^2-10^3 nm range, are compatible with those obtained in bulk measurements.[19]

The temperature rise as a function of the power in the trap is studied in Fig. 4. It is observed that the experimental measurement was always lower than the theoretical prediction at the surface of one NP ($r = R$) considering the mild heating from water absorption (some 0.3 K at 100 mW within the focal region, see previous subsection). Then, it is clear that the Stokes' law assays access the water temperature in an environment around the trapped IONP@SiO_2 nanostructure instead of directly on the SiO_2 outer surface. After including the effect of water absorption, theory and experiment nearly coincide at $r = 57$ nm, i.e. some 7 nm away from the outer surface of the IONP@SiO_2 nanostructure. This implies that temperature measurements

comply with an energy equivalent to the kinetic motion of water molecules averaged over some 30 molecular layers.

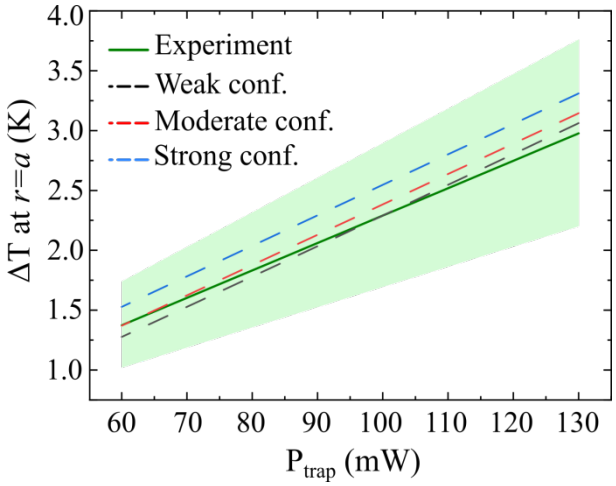

Figure 4. Temperature as a function of the laser power. The temperature rise near a single optically-trapped IONP@SiO_2 nanostructure is shown (green curve and shaded area, mean ± SD), together with the theoretical predictions at $r = a$ for weak (black), moderate (red) and strong (blue) confinement regimes (Supporting Information).

In conclusion, we have measured for the first time the temperature near an individual heating NP by a fundamental method, that is, without the use of neighboring nanostructures calibrated for temperature sensing, which may alter the physical properties of the heating NP. To that end, we have used an optical trap to confine the NP and induce its heating through optical absorption. We have developed straightforward theoretical methods to interpret the temperature measurements, which take into account the Brownian motion of the NP in the trap. This theory can be used to predict temperature gradients by other optically absorbing nanostructures manipulated by laser tweezers in the limit of very small particles, where optical heating becomes stochastic. From the point of view of the use of NPs in biomedicine, a spatial change in

temperature, which does not necessarily involve a high temperature maximum, may dramatically alter signaling pathways that lead to cell death.

Theory and experiments confirm IONPs as efficient optical heat generators over metallic NPs away from plasmon resonance conditions. We have used a low power NIR laser, which enables non-invasive radiation for optical hyperthermia thus pushing forward the versatility of IONPs in health. More in depth, beyond their use in contrast imaging, our results with IONP@SiO_2 nanostructures show that optical hyperthermia implemented with NIR lasers generates temperatures similar to those obtained by magnetic hyperthermia under AC magnetic fields in the MHz. These methods are physically independent and biologically compatible, and, therefore, they may be simultaneously tuned to optimize the heating response of IONPs at specific biomedical scenarios. Finally, we present silica-coating as a chemical route to increase optical absorption and thus the heating capacity of IONPs in physiological media, a strategy that is also convenient for their optical tweezing under weak laser focusing.

Temperature is a physical property that makes sense on average over the many-body dynamics of the materials' components. Extending this statistic concept down to the nanoscale is challenging because the number of these components may be limited, especially when the heating source is small and subjected to collisions with them. Our results shed light on the understanding of temperature microscopically and for general non-equilibrium problems. In particular, by comparing theory and experiments, we show that the temperature outside a heating NP corresponds to the average kinetic energy of a few tens of water molecule layers.

ASSOCIATED CONTENT

Supporting Information. Experimental section, nanostructure sample characterization, luminescence of optically trapped silica-coated magnetic nanostructures, behavior of a single

nanostructure in the optical trap, heat equation for silica-coated magnetic nanostructures, power absorbed by an optically trapped nanostructure, relation between the power in the trap and the power absorbed by a nanostructure, hydrodynamic diameter and laser heating factor of optically trapped nanostructures: Raw data, and temperature rise due to water absorption.

ACKNOWLEDGMENT

Work supported by the Spanish Ministry of Science, Innovation and Universities (grant MAT2015-71806-R). IMDEA Nanociencia acknowledges support from the "Severo Ochoa" Programme for Centers of Excellence in R&D (SEV-2016-0686). H.R-R. is supported by an FPI-UAM 2015 fellowship.

REFERENCES

1. Mohammed, L.; Gomaa, H. G.; Ragab, D.; Zhu, J. Magnetic nanoparticles for environmental and biomedical applications: A review. *Particuology* **2017**, *30*, 1-14.

2. Beik, J.; Abed, Z.; Ghoreishi, F. S.; Hosseini-Nami, S.; Mehrzadi, S.; Shakeri-Zadeh, A.; Kamrava, S. K. Nanotechnology in hyperthermia cancer therapy: From fundamental principles to advanced applications. *J. Control. Release* **2016**, *235*, 205-221.

3. Jaque, D.; Maestro, L. M.; Rosal, B. D.; Haro-Gonzalez, P.; Benayas, a.; Plaza, J. L.; Rodríguez, E. M.; Solé, J. G. Nanoparticles for photothermal therapies. *Nanoscale* **2014**, *6*, 9494-9530.

4. Ling, D.; Lee, N.; Hyeon, T. Chemical Synthesis and Assembly of Uniformly Sized Iron Oxide Nanoparticles for Medical Applications. *Acc. Chem. Res.* **2015**, *48*, 1276-1285.

5. Stanicki, D.; Elst, L. V.; Muller, R. N.; Laurent, S. Synthesis and processing of magnetic nanoparticles. *Curr. Opin. Chem. Eng.* **2015**, *8*, 7-14.

6. Jin, R.; Lin, B.; Li, D.; Ai, H. Superparamagnetic iron oxide nanoparticles for MR imaging and therapy: design considerations and clinical applications. *Curr. Opin. Pharmacol.* **2014**, *18*, 18-27.

7. Singh, D.; McMillan, J. M.; Kabanov, A. V.; Sokolsky-Papkov, M.; Gendelman, H. E. Bench-to-bedside translation of magnetic nanoparticles. *Nanomedicine* **2014**, *9*, 501-516.

8. Weissig, V.; Pettinger, T. K.; Murdock, N. Nanopharmaceuticals (part 1): products on the market. *Int. J. Nanomed.* **2014**, *9*, 4357-4373.

9. Mosayebi, J.; Kiyasatfar, M.; Laurent, S. Synthesis, Functionalization, and Design of Magnetic Nanoparticles for Theranostic Applications. *Adv. Healthc. Mater.* **2017**, *6*, 1700306.

10. Shen, S.; Kong, F.; Guo, X.; Wu, L.; Shen, H.; Xie, M.; Wang, X.; Jin, Y.; Ge, Y. CMCTS stabilized Fe3O4 particles with extremely low toxicity as highly efficient near-infrared photothermal agents for in vivo tumor ablation. *Nanoscale* **2013**, *5*, 8056-8066.

11. Espinosa, A.; Di Corato, R.; Kolosnjaj-Tabi, J.; Flaud, P.; Pellegrino, T.; Wilhelm, C. Duality of Iron Oxide Nanoparticles in Cancer Therapy: Amplification of Heating Efficiency by Magnetic Hyperthermia and Photothermal Bimodal Treatment. *ACS Nano* **2016**, *10*, 2436-2446.

12. Chen, H.; Burnett, J.; Zhang, F.; Zhang, J.; Paholak, H.; Sun, D. Highly crystallized iron oxide nanoparticles as effective and biodegradable mediators for photothermal cancer therapy. *J. Mater. Chem. B* **2014**, *2*, 757-765.

13. Liao, M.-Y.; Lai, P.-S.; Yu, H.-P.; Lin, H.-P.; Huang, C.-C. Innovative ligand-assisted synthesis of NIR-activated iron oxide for cancer theranostics. *Chem. Commun.* **2012**, *48*, 5319-5321.

14. Zhou, Z.; Sun, Y.; Shen, J.; Wei, J.; Yu, C.; Kong, B.; Liu, W.; Yang, H.; Yang, S.; Wang, W. Iron/iron oxide core/shell nanoparticles for magnetic targeting MRI and near-infrared photothermal therapy. *Biomaterials* **2014**, *35*, 7470-7478.

15. Shen, S.; Wang, S.; Zheng, R.; Zhu, X.; Jiang, X.; Fu, D.; Yang, W. Magnetic nanoparticle clusters for photothermal therapy with near-infrared irradiation. *Biomaterials* **2015**, *39*, 67-74.

16. Wang, J.; Zhao, H.; Zhou, Z.; Zhou, P.; Yan, Y.; Wang, M.; Yang, H.; Zhang, Y.; Yang, S. MR/SPECT Imaging Guided Photothermal Therapy of Tumor-Targeting Fe@Fe3O4 Nanoparticles in Vivo with Low Mononuclear Phagocyte Uptake. *ACS Appl. Mater. Interfaces* **2016**, *8*, 19872-19882.

17. Chu, M.; Shao, Y.; Peng, J.; Dai, X.; Li, H.; Wu, Q.; Shi, D. Near-infrared laser light mediated cancer therapy by photothermal effect of Fe3O4 magnetic nanoparticles. *Biomaterials* **2013**, *34*, 4078-4088.

18. Peng, H.; Tang, J.; Zheng, R.; Guo, G.; Dong, A.; Wang, Y.; Yang, W. Nuclear-Targeted Multifunctional Magnetic Nanoparticles for Photothermal Therapy. *Adv. Healthc. Mater.* **2017**, *6*, 1601289.

19. Ortgies Dirk, H.; Teran Francisco, J.; Rocha, U.; de la Cueva, L.; Salas, G.; Cabrera, D.; Vanetsev Alexander, S.; Rähn, M.; Sammelselg, V.; Orlovskii Yurii, V.; Jaque, D. Optomagnetic Nanoplatforms for In Situ Controlled Hyperthermia. *Adv. Funct. Mater.* **2018**, *28*, 1704434.

20. Ren, X.; Zheng, R.; Fang, X.; Wang, X.; Zhang, X.; Yang, W.; Sha, X. Red blood cell membrane camouflaged magnetic nanoclusters for imaging-guided photothermal therapy. *Biomaterials* **2016**, *92*, 13-24.

21. Hemmer, E.; Venkatachalam, N.; Hyodo, H.; Hattori, A.; Ebina, Y.; Kishimoto, H.; Soga, K. Upconverting and NIR emitting rare earth based nanostructures for NIR-bioimaging. *Nanoscale* **2013**, *5*, 11339-11361.

22. Anderson, R. R.; Parrish, J. A. The Optics of Human Skin. *J. Invest. Dermatol.* **1981**, *77*, 13-19.

23. Southern, P.; Pankhurst, Q. A. Commentary on the clinical and preclinical dosage limits of interstitially administered magnetic fluids for therapeutic hyperthermia based on current practice and efficacy models. *Int. J. Hyperther.* **2018**, *34*, 671-686.

24. Dias Jorge, T.; Moros, M.; del Pino, P.; Rivera, S.; Grazú, V.; de la Fuente Jesus, M. DNA as a Molecular Local Thermal Probe for the Analysis of Magnetic Hyperthermia. *Angew. Chem. Int. Ed.* **2013**, *52*, 11526-11529.

25. Riedinger, A.; Guardia, P.; Curcio, A.; Garcia, M. A.; Cingolani, R.; Manna, L.; Pellegrino, T. Subnanometer Local Temperature Probing and Remotely Controlled Drug Release Based on Azo-Functionalized Iron Oxide Nanoparticles. *Nano Lett.* **2013**, *13*, 2399-2406.

26. Piñol, R.; Brites, C. D. S.; Bustamante, R.; Martínez, A.; Silva, N. J. O.; Murillo, J. L.; Cases, R.; Carrey, J.; Estepa, C.; Sosa, C.; Palacio, F.; Carlos, L. D.; Millán, A. Joining Time-Resolved Thermometry and Magnetic-Induced Heating in a Single Nanoparticle Unveils Intriguing Thermal Properties. *ACS Nano* **2015**, *9*, 3134-3142.

27. Bendix, P. M.; Reihani, S. N. S.; Oddershede, L. B. Direct Measurements of Heating by Electromagnetically Trapped Gold Nanoparticles on Supported Lipid Bilayers. *ACS Nano* **2010**, *4*, 2256-2262.

28. Urban, A. S.; Fedoruk, M.; Horton, M. R.; Rädler, J. O.; Stefani, F. D.; Feldmann, J. Controlled Nanometric Phase Transitions of Phospholipid Membranes by Plasmonic Heating of Single Gold Nanoparticles. *Nano Lett.* **2009**, *9*, 2903-2908.

29. Rodríguez-Rodríguez, H.; de Lorenzo, S.; de la Cueva, L.; Salas, G.; Arias-Gonzalez, J. R. Optical Trapping of Single Nanostructures in a Weakly Focused Beam. Application to Magnetic Nanoparticles. *J. Phys. Chem. C* **2018**, *122*, 18094-18101.

30. van de Hulst, H. C. Light Scattering by Small Particles. 3 ed.; Dover: New York, **1981**.

31. Schlegel, A.; Alvarado, S. F.; Wachter, P. Optical properties of magnetite (Fe3O4). *J. Phys. C: Solid State Phys.* **1979**, *12*, 1157.

32. Johnson, P. B.; Christy, R. W. Optical Constants of the Noble Metals. *Phys. Rev. B* **1972**, *6*, 4370-4379.

33. Hormeno, S.; Gregorio-Godoy, P.; Perez-Juste, J.; Liz-Marzan, L. M.; Juarez, B. H.; Arias-Gonzalez, J. R. Laser heating tunability by off-resonant irradiation of gold nanoparticles. *Small* **2014**, *10*, 376-84.

34. Aden, A. L.; Kerker, M. Scattering of Electromagnetic Waves from Two Concentric Spheres. *J. Appl. Phys.* **1951**, *22*, 1242-1246.

35. Bohren, C. F.; Huffman, D. R. Absorption and Scattering of Light by Small Particles. Wiley-Interscience Publication: New York, **1983**.

36. Kerker, M. The Scattering of light and Other Electromagnetic Radiation. Academic Press: New York, **1969**.

37. De Lorenzo, S.; Ribezzi-Crivellari, M.; Arias-Gonzalez, J. R.; Smith, S. B.; Ritort, F. A Temperature-Jump Optical Trap for Single-Molecule Manipulation. *Biophys. J.* **2015**, *108*, 2854-2864.

38. Hormeño, S.; Bastús, N. G.; Juárez, B. H.; Pietsch, A.; Weller, H.; Arias-Gonzalez, J. R. Plasmon-Exciton Interactions on Single Thermoresponsive Platforms Demonstrated by Optical Tweezers. *Nano Lett.* **2011**, *11*, 4742-4747.

39. Rodriguez-Rodriguez, H.; Acebron, M.; Juarez, B. H.; Ricardo Arias-Gonzalez, J. Luminescence Dynamics of Silica-Encapsulated Quantum Dots During Optical Trapping. *J. Phys. Chem. C* **2017**, *121*, 10124-10130.

40. Hormeno, S.; Ibarra, B.; Chichon, F. J.; Habermann, K.; Lange, B. M.; Valpuesta, J. M.; Carrascosa, J. L.; Arias-Gonzalez, J. R. Single centrosome manipulation reveals its electric charge and associated dynamic structure. *Biophys. J.* **2009**, *97*, 1022-30.

41. Mao, H.; Arias-Gonzalez, J. R.; Smith, S. B.; Tinoco, I.; Bustamante, C. Temperature control methods in a laser tweezers system. *Biophys. J.* **2005**, *89*, 1308-16.

42. Peterman, E. J. G.; Gittes, F.; Schmidt, C. F. Laser-induced heating in optical traps. *Biophys. J.* **2003**, *84*, 1308-1316.

43. Català, F.; Marsà, F.; Montes-Usategui, M.; Farré, A.; Martín-Badosa, E. Influence of experimental parameters on the laser heating of an optical trap. *Sci. Rep.* **2017**, *7*, 16052.

44. Govorov, A. O.; Zhang, W.; Skeini, T.; Richardson, H.; Lee, J.; Kotov, N. a. Gold nanoparticle ensembles as heaters and actuators: Melting and collective plasmon resonances. *Nanoscale Res. Lett.* **2006**, *1*, 84-90.